DIMUON PRODUCTION BY HIGH ENERGY NEUTRONS

E 87/358

BY

CLYDE DEAN WHEELER

B. S., Southwestern State College, 1960
M. S. T., Cornell University, 1966
M. S., University of Illinois, 1971

THESIS

Submitted in partial fulfillment of the requirements
for the degree of Doctor of Philosophy in Physics
in the Graduate College of the
University of Illinois at Urbana-Champaign, 1976

Urbana, Illinois

FERMILAB
LIBRARY

DIMUON PRODUCTION BY HIGH ENERGY NEUTRONS

Clyde Dean Wheeler, Ph.D.
Department of Physics
University of Illinois at Urbana-Champaign, 1976

In the broad band neutral beam at Fermi National Accelerator Laboratory, the dimuon production by high energy neutrons has been measured for incident neutron energies of approximately 250 and 320 GeV. The mass spectra show clear peaks in the rho-omega mass region and at the J/psi mass. Cross sections and longitudinal and transverse momenta distributions are given for the J/psi. The data between 1.0 and 3.0 GeV/c^2 are compared with the mass distribution predicted by the Drell-Yan model.

ACKNOWLEDGMENTS

Experiments of this magnitude necessarily involve a large number of people. Although space does not permit me to thank all of them individually, I would like to express my graditude to all who have contributed directly or indirectly to this experiment.

I am especially indebted to my advisor, Professor T. O'Halloran, for his interest, advice, guidance, and friendship throughout my graduate career at the University of Illinois.

Professor A. Wattenberg provided valuable advice and guidance, particularly in regard to apparatus design and construction, and his continued interest is appreciated. I am grateful to Professors M. Gormley and G. Gladding for many valuable discussions and for their significant contributions to this work.

I am indebted to my fellow graduate students, J. Bronstein, L. Cormell, and J. Sarracino for their hard work, useful discussions, and friendship during the course of this experiment.

From the beginning, the experiment depended on an extensive group effort. I would like to thank the members of the group for their dedication and hard work in planning, setting up, and running the experiment and in analyzing the data. In addition to those already mentioned, the members of the group are: Professor W. Lee, Dr. B. Knapp, P. Leung, D. Smith, and A. Wijangco from Columbia University; Dr. R. Messner and R. Coleman from the University of

Illinois; Dr. M. Binkley, Dr. I. Gaines, Dr. R. Orr, Dr. J. Peoples, and Dr. L. Read from the Fermi National Accelerator Laboratory; Dr. D. Yount and J. Knauer from the University of Hawaii; and D. Nease from Cornell University.

I would like to thank the staff of the PDP-10 for their assistance, the technical staff for their contributions to the design and construction of the apparatus, and the staff of the Fermi National Accelerator Laboratory for their support. Our technician, L. Seward, did his usual excellent work.

This research was supported in part by the U. S. Atomic Energy Commission under contract AT(11-1)-1195.

TABLE OF CONTENTS

		Page
I.	INTRODUCTION	1
II.	DESCRIPTION OF THE EXPERIMENT	4
	A. Neutral Beam	4
	B. Experimental Layout	6
	C. Data Acquisition System	11
	D. Electronics and Logic	14
III.	ANALYSIS	22
	A. Data Reduction	22
	B. Muon Identification	23
	C. Mass Calculation	24
	D. Monte Carlo Event Simulation	26
	E. Normalization	27
	F. Drell-Yan Calculation	29
IV.	RESULTS	30
	A. Mass Distributions	30
	B. J/Psi(3100)	35
	C. Dimuon Continuum	41
	D. Psi'(3700)	41
V.	SUMMARY	44
	REFERENCES	45
	VITA	46

I. INTRODUCTION

An experiment was conducted at the Fermi National Accelerator Laboratory to study the dimuon production by high energy neutrons. Preliminary data taken in September, 1974, demonstrated the feasibility of the experimental method and showed the presence of a dimuon signal. The data for this thesis were obtained in two short runs in November, 1974, and March, 1975. Some of the results from the November run have been published.[1]

The initial motivation for the experiment was provided by the observation of prompt leptons at large transverse momentum in hadronic interactions.[2-5] Any understanding of this single lepton production certainly requires at least some information about the dilepton production. Of particular interest with respect to the single leptons are the production of high mass dimuons and the production of low mass dimuons at high transverse momentum. With the discovery of the narrow resonances that couple to the dilepton state,[6-9] the emphasis of the experiment shifted to the study of the production of these resonances by high energy neutrons.

Virtual photon processes certainly contribute to the direct production of dileptons in hadronic interactions. Figure 1a shows the general diagram for such processes. If we accept the traditional belief that leptons have only electromagnetic and weak interactions, these are probably the dominant sources of the prompt dimuons. The leptonic

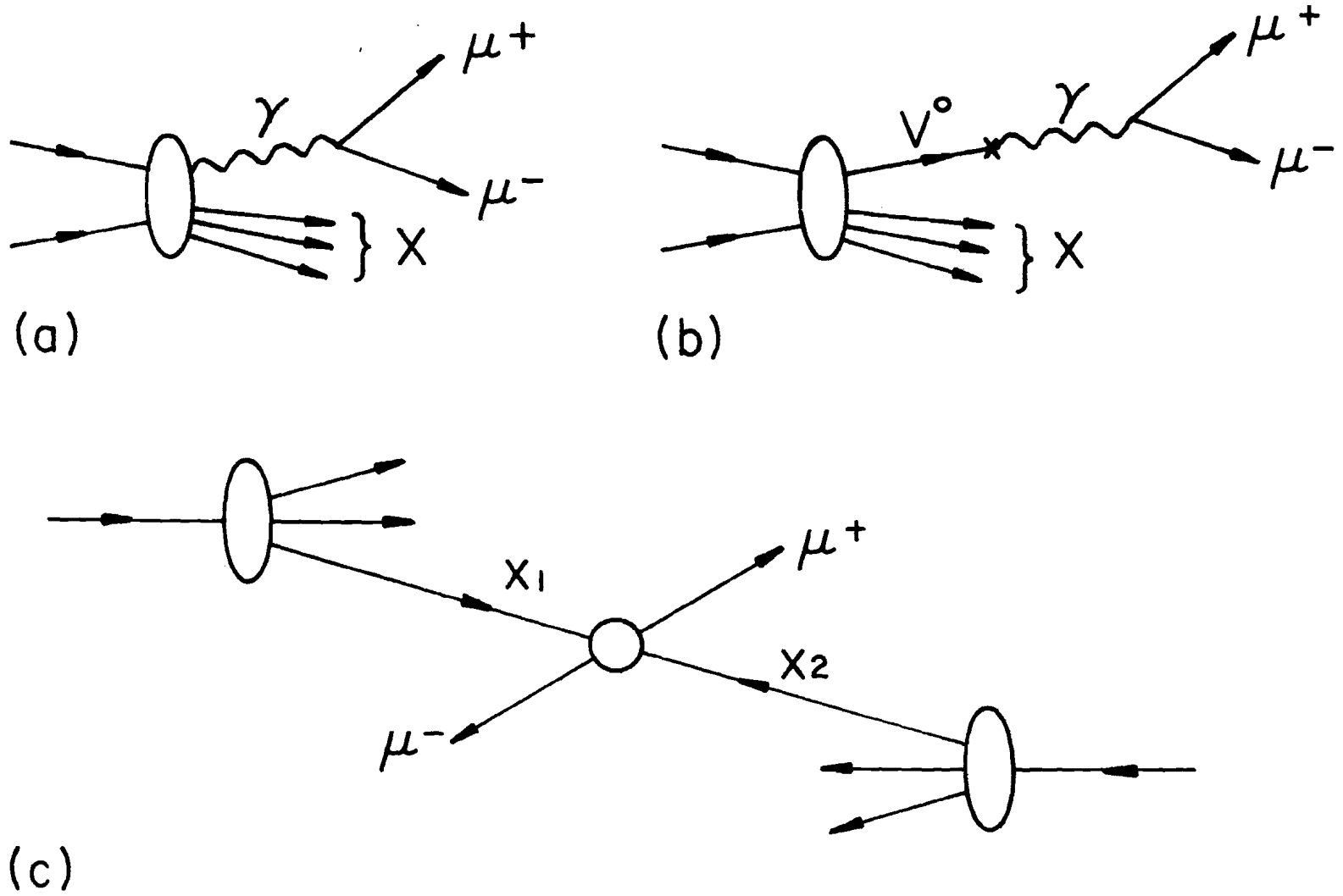

Figure 1. Dimuon production by virtual photon processes: (a) the general diagram; (b) the leptonic decay of vector mesons; (c) the Drell-Yan parton-antiparton annihilation mechanism.

decay of vector mesons, figure 1b, is one such process that gives discrete dilepton masses. The data show that this process is a significant, if not the dominant, source of the dimuons observed in this experiment.

A mechanism for the production of a massive dilepton continuum[10] has been proposed by Drell and Yan.[11] The Drell-Yan parton-antiparton annihilation process is shown in figure 1c. Internal conversion for processes producing real photons, such as Bremsstrahlung or gamma decays of hadrons, would also contribute to the dimuon continuum but would be peaked toward the lower end of the mass spectrum.

The emphasis of this thesis is on the higher mass dimuons. The experimental setup and data collection system are described in section II. Section III describes the data reduction and other features of the data analysis. The experimental results are discussed in section IV and summarized in section V.

II. DESCRIPTION OF THE EXPERIMENT

A. Neutral Beam

The experiment was performed in the broad band, zero milliradian, neutral beam in the Proton East beam line at the Fermi National Accelerator Laboratory. The neutral beam was generated by protons incident on a 30.5 cm beryllium target. Data were taken with incident proton momenta of 300 GeV/c in November, 1974, and 380 GeV/c in March, 1975.

The neutral beam layout is shown in figure 2. Immediately downstream of the target, sweeping magnets swept the non-interacting protons and charged secondaries into a tungsten and magnetized steel beam dump. A 13 mm diameter hole through the dump allowed the neutral beam to pass through a series of collimators and sweeping magnets. The neutral beam spot size was approximately 1.5 cm by 1.5 cm at the experimental target.

In the magnet immediately upstream of the second collimator, six pieces of 6.4 mm thick lead were remotely inserted into the beam to attenuate the photon component. This lead was spaced in the magnetic field to prevent the build-up of electromagnetic cascades. For the run with 380 GeV/c protons an additional 7.6 cm of lead was placed upstream of this magnet to attenuate further the photons.

The neutron spectrum was measured by absorbing low intensity neutral beam in a hadron calorimeter counter. This counter consisted

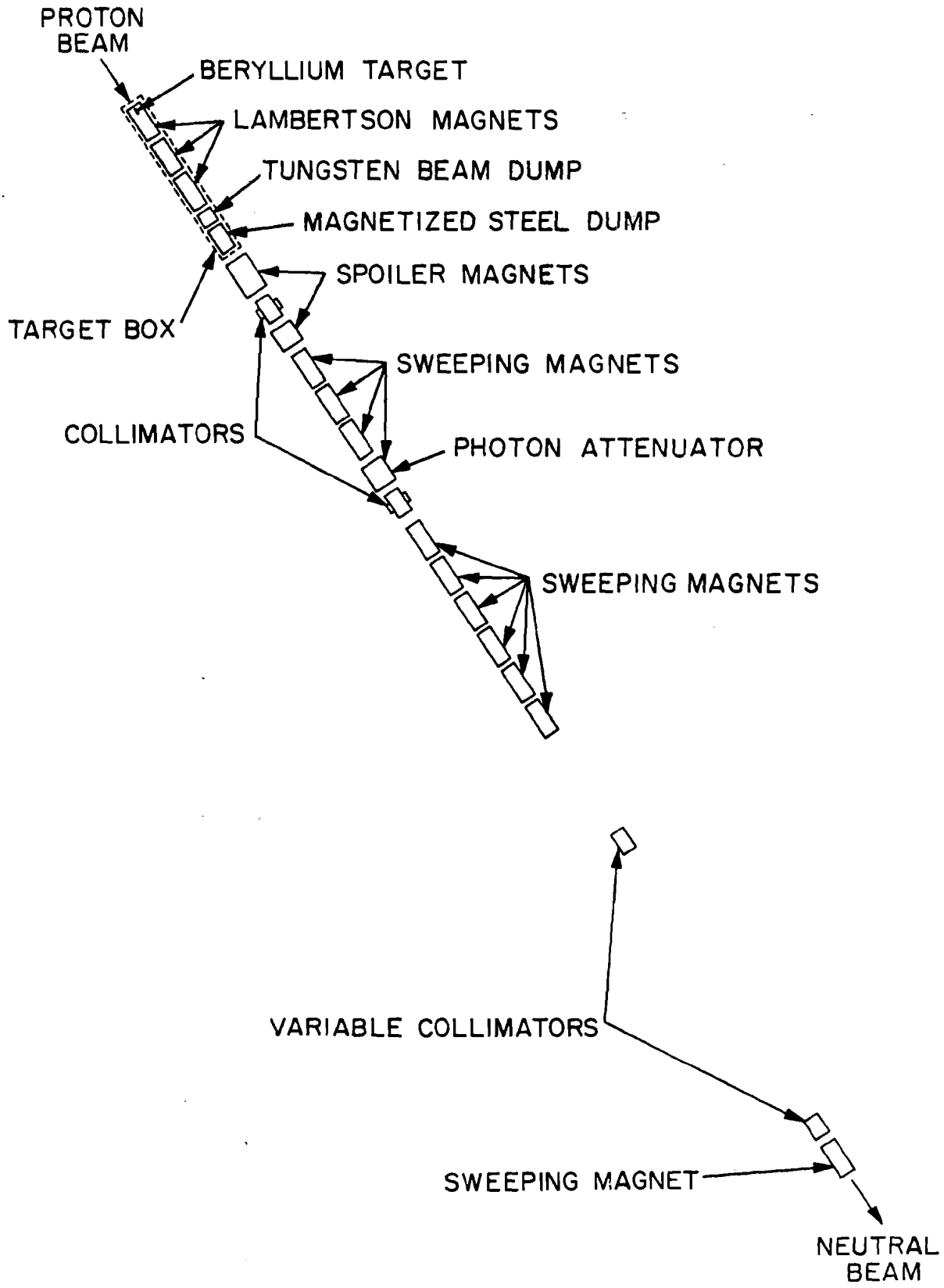

Figure 2. Neutral beam layout

of twelve layers of 6.4 mm thick plastic scintillator interspersed with 5.1 cm thick steel sheets. The scintillator was viewed by a single phototube. The energy resolution of this counter was measured to be ±50% in a 50 GeV pion beam. The neutron energy spectra are shown in figure 3. The spectrum for the November run with 300 GeV protons shows the energy spectrum of the full neutral beam as measured in the hadron calorimeter. For the March run with 380 GeV protons, the hadron calorimeter consisted of two counters centered 10 cm above the beam line. The spectrum for this run includes only those events for which a measurable amount of energy was deposited in both counters.

B. Experimental Layout

The experimental layout is shown in figure 4. The detector consisted of a multiwire proportional chamber magnetic spectrometer and a particle identification system. Upstream of the target there was an array of anti-counters (A) to veto charged particles in the neutral beam and muons from upstream sources. Trigger counters (B) were centered on the beam line downstream of the target. Downstream of the magnetic spectrometer there were two planes of trigger counters, a horizontal array (H) of twelve counters and a vertical array (V) of eight counters.

The target configurations used for the two runs are shown in figure 5. For the November run the target consisted of an upstream target of 1.8 cm thick beryllium followed by a target monitor counter (B1) and a downstream target. Downstream targets of 22.9, 15.2, and

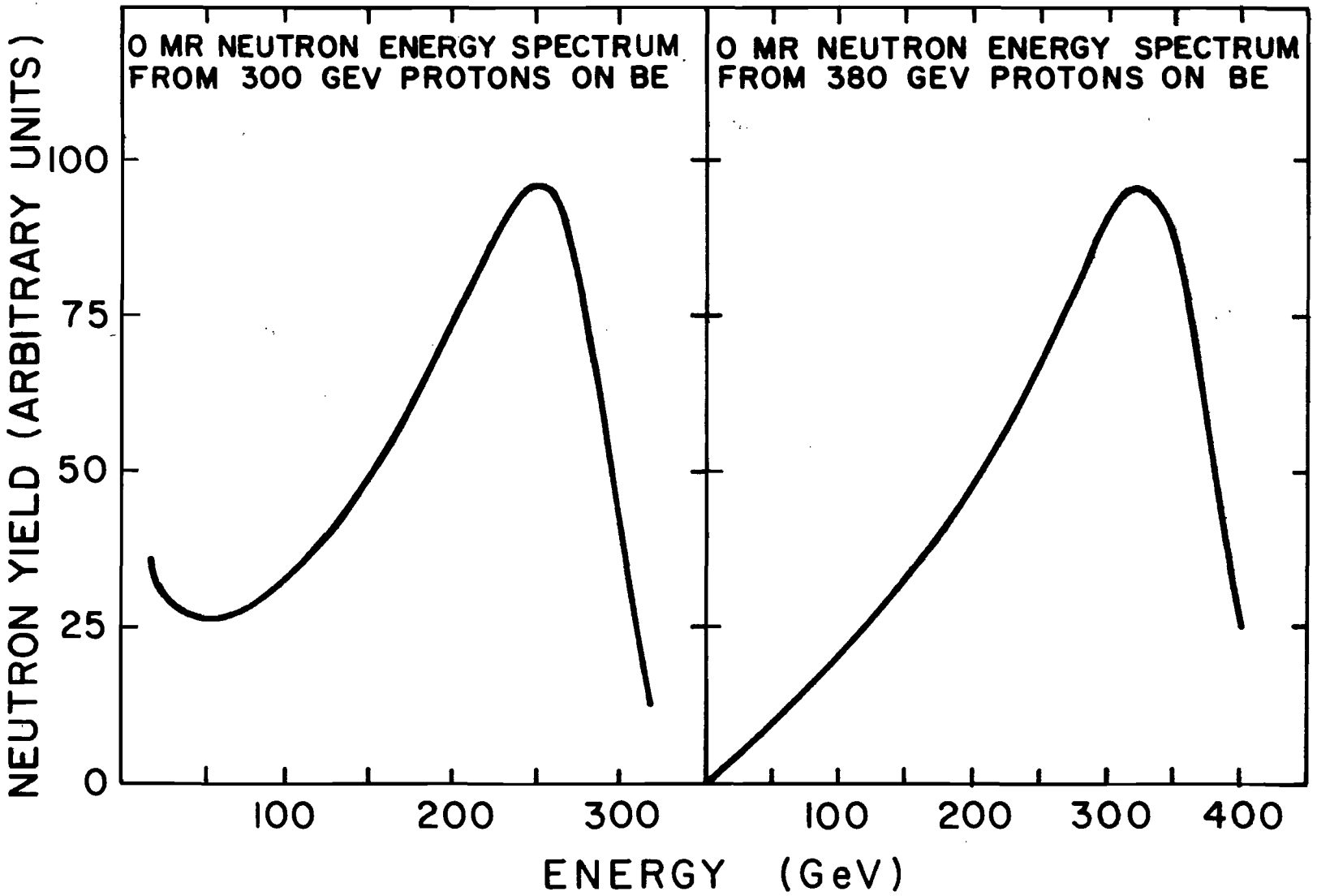

Figure 3. Neutron energy spectra

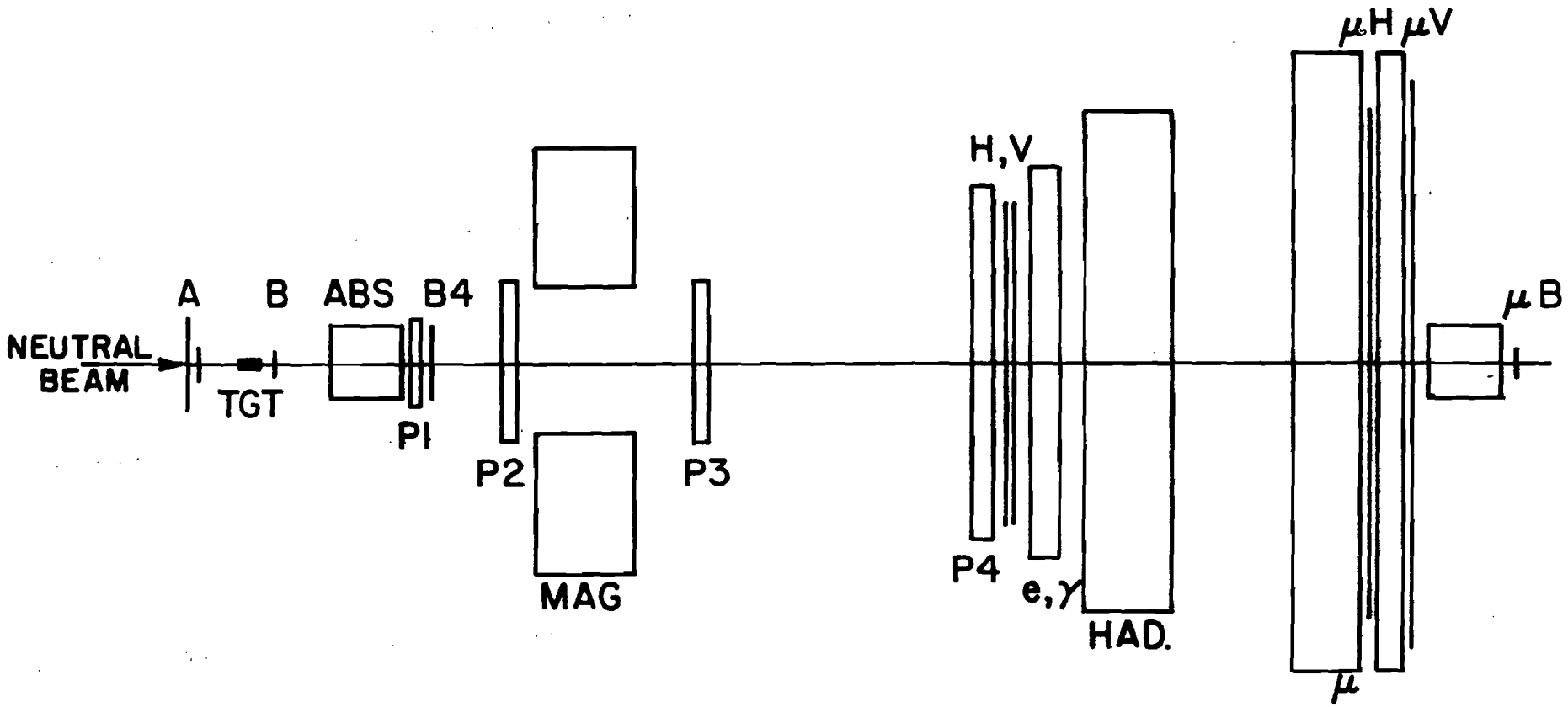

Figure 4. Experimental layout

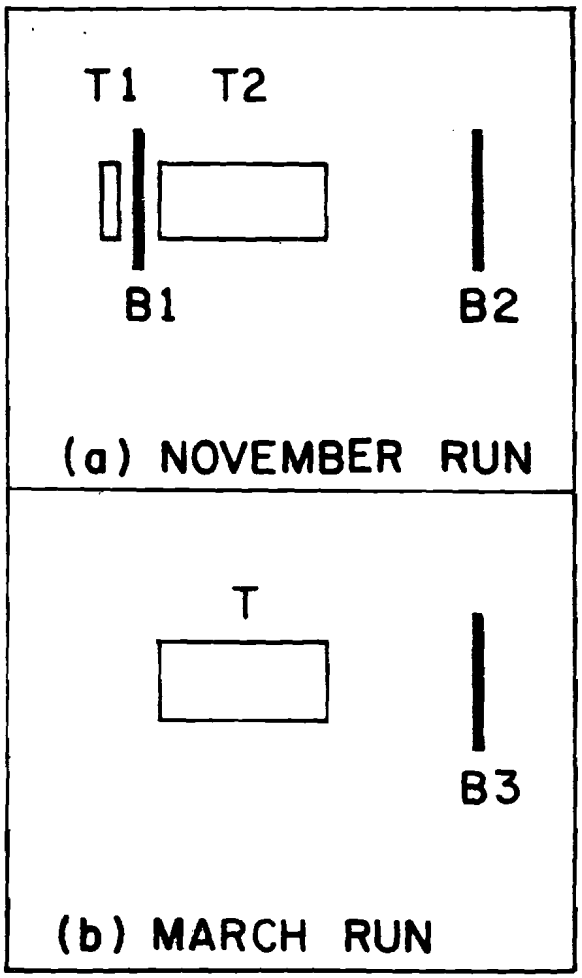

Figure 5. Target configurations

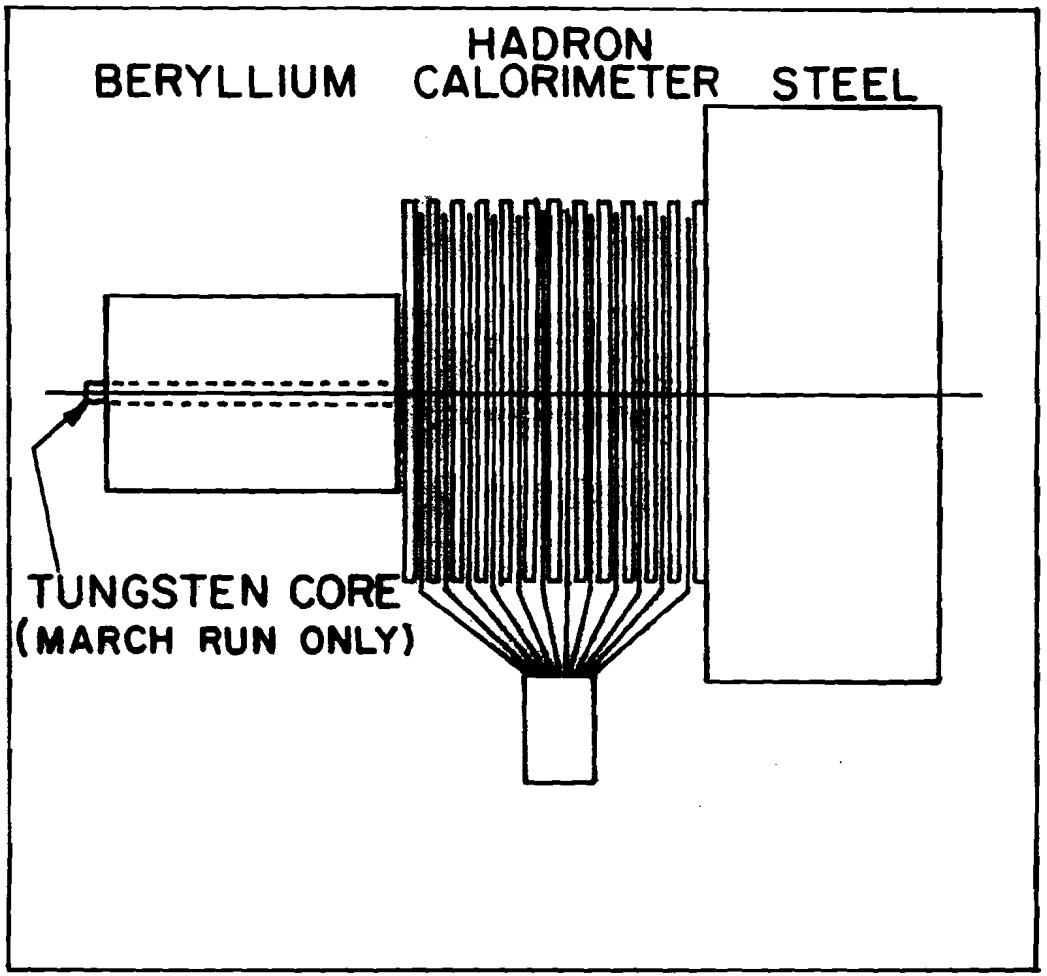

Figure 6. Absorber

7.6 cm of beryllium were used. The upstream target was removed for most of the data taken with the 15.2 cm downstream target. For the March run targets of 7.6 and 15.2 cm of beryllium were used. The counters downstream of the targets (B2, B3) were used to identify events in which an interaction occurred in the target. They also served as target monitors by counting the total number of target interactions. Typical counting rates for these counters were 1.5 to 2.0 x 10^6 per pulse.

An absorber was placed downstream of the target to attenuate the interaction products other than muons and to reduce the decay path for pions and kaons produced in the target. It also served as a beam dump for the non-interacting neutral beam. The absorber consisted of 58 cm of beryllium and 190 cm of steel for the November run and 81 cm of beryllium and 127 cm of steel for the March run. Its general structure is shown in figure 6. For the March run the beryllium portion of the absorber had a 2.5 cm diameter tungsten core centered on the beam line. For both runs the upstream 66 cm of steel included the hadron calorimeter that was used to measure the neutron spectrum. The beryllium sections of the absorbers were removed for the neutron spectrum measurements.

The magnetic spectrometer used four multiwire proportional chambers with two upstream and two downstream of the spectrometer magnet. Each proportional chamber had three planes, an x plane with vertical wires and u and v planes with wires at angles of 11.3° from

the horizontal. All wire spacings were 2.0 mm except for the vertical wires in the large downstream chamber which had a 3.0 mm spacing. There were a total of approximately 4400 wires in the four chambers.

The vertically bending spectrometer magnet had a field integral of 0.60 GeV/c per unit charge. The acceptance of the spectrometer was determined by the magnet aperture which was 41 cm horizontally by 61 cm vertically. The momentum resolution of the spectrometer was approximately 5% (rms) at 100 GeV/c.

With the upstream absorber the particle identification system provided only muon identification. As a muon identifier, it consisted of 14 cm of lead and 240 cm of steel, a horizontal array of twenty-two muon counters, an additional 64 cm of steel, and a vertical array of eighteen muon counters. Since there was a 15 cm by 15 cm hole through part of the steel and a 15 cm by 20 cm gap in the horizontal array of muon counters, an additional 100 cm of steel and an additional counter were centered on the beam line to provide better identification of the energetic muons that remained near the beam line.

C. Data Acquisition System

A block diagram of the data acquisition system is shown in figure 7. A "master gate" (MG) or input trigger was generated with fast logic from the discriminator outputs from the trigger counters. This master gate was sent to the input trigger generator (TGI) which cleared the coincidence registers (CR) and gated the event into the coincidence

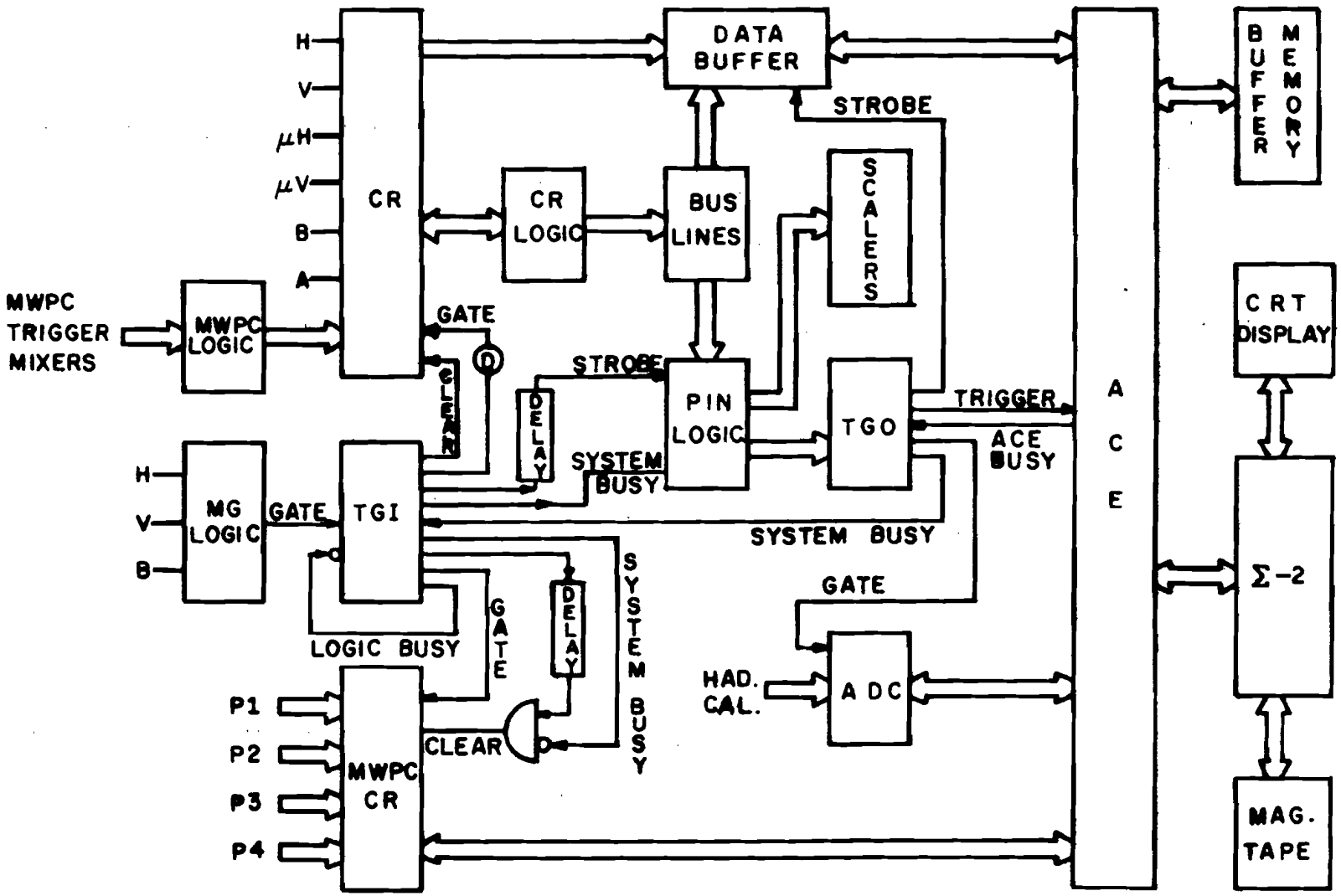

Figure 7. Block diagram of the data acquisition system

registers. Once the event was stored in the coincidence registers, all further logical operations were done with D. C. logic.

Within the CR logic system, up to sixteen logical definitions were derived and distributed to a data bus. Logic modules in the pin logic system defined event classifications according to internal, pre-set switch connections to this data bus. The pin logic modules were strobed and produced output pulses for direct scaling and output triggers which were mixed in the output trigger generator (TGO) to form the event trigger. With the event trigger the output trigger generator produced gates for the pulse height digitizers and a strobe for the data buffer system to store and save the event data for the readout system.

Each time an input trigger was accepted, a logic deadtime was generated by the input trigger generator to prevent the acceptance of input triggers during the time required to propagate the logic, form output triggers, and store the event in the data buffers. If the input trigger produced an event trigger, a system deadtime was generated by the output trigger generator and extended by the event readout system to cover the time required to transfer the event data to the buffer memory. This system deadtime prevented the generation of output triggers and the "clear" and "gate" signals for the proportional chamber coincidence registers. Except for the generation of output triggers, the entire logic system was available to continue processing and scaling events during the data readout process. The system deadtime was measured

with the same logic system that triggered the accepted events.

The event trigger signaled the data transfer controller (ACE) to start the readout process. ACE responded with "ACE Busy" which extended the system deadtime. The event data were read in sequence and stored in a 32K buffer memory. When the data transfer was completed, "ACE Busy" was brought down and the system was ready to accept another event. This process continued until the buffer memory was full or until an end-of-spill signal was received. With a full buffer memory ACE would hold the "ACE Busy" until the end-of-spill, and no further output triggers would be generated during that spill. When an end-of-spill signal was received, an interrupt was sent to the Sigma-2 computer which read in the events from the buffer memory, tagged each event, and wrote the events on magnetic tape.

In addition, the Sigma-2 read the monitor scalars and accumulated event statistics for each spill and wrote the information on magnetic tape. This information was also accumulated for the full run, and the totals were printed out at the end of the run. The computer also analyzed a sample of the events during the run. Various distributions and individual events could be viewed on the on-line CRT display unit.

D. Electronics and Logic

For the March run the master gate was derived from the H, V trigger counters. It required at least one counter from one plane with at least two counters from the other plane. This (H, V >1) logic is

shown in figure 8a. For the November run the upstream trigger counters B2 and B4 were also required as shown in figure 8b. The master gate was $B2 \cdot B4 \cdot (H, V > 1)$ for the November run and $(H, V > 1)$ for the March run.

The amplifier cards for the multiwire proportional chambers readout system accepted eight wire signals and provided the outputs that went to the MWPC coincidence registers. In addition, each card also provided an "OR" of all eight signals. These "OR" or trigger mixer signals were the input signals for the MWPC logic system.

Figure 9a shows the P1 logic which required at least one hit in two or more of the three planes in P1. This logic was required in both runs to eliminate potential triggers which could not possibly produce reconstructable tracks. Figure 9b shows the P3 logic used in the November run to improve further the two particle trigger by requiring hits in at least two of the four quadrants of P3.

Figure 9c shows the two particle, wide angle track logic used in the March run. It required more than one hit in two or more planes of both P2 and P3. In addition, the "sum unit" had been modified to provide separate OR circuits for the left and right halves of the x planes of P2 and P3. By removing a central band of wires from these OR circuits, hits were required outside and to the right (or left) of the central region of both chambers. This "wide angle track" requirement favored events of high mass or large transverse momentum.

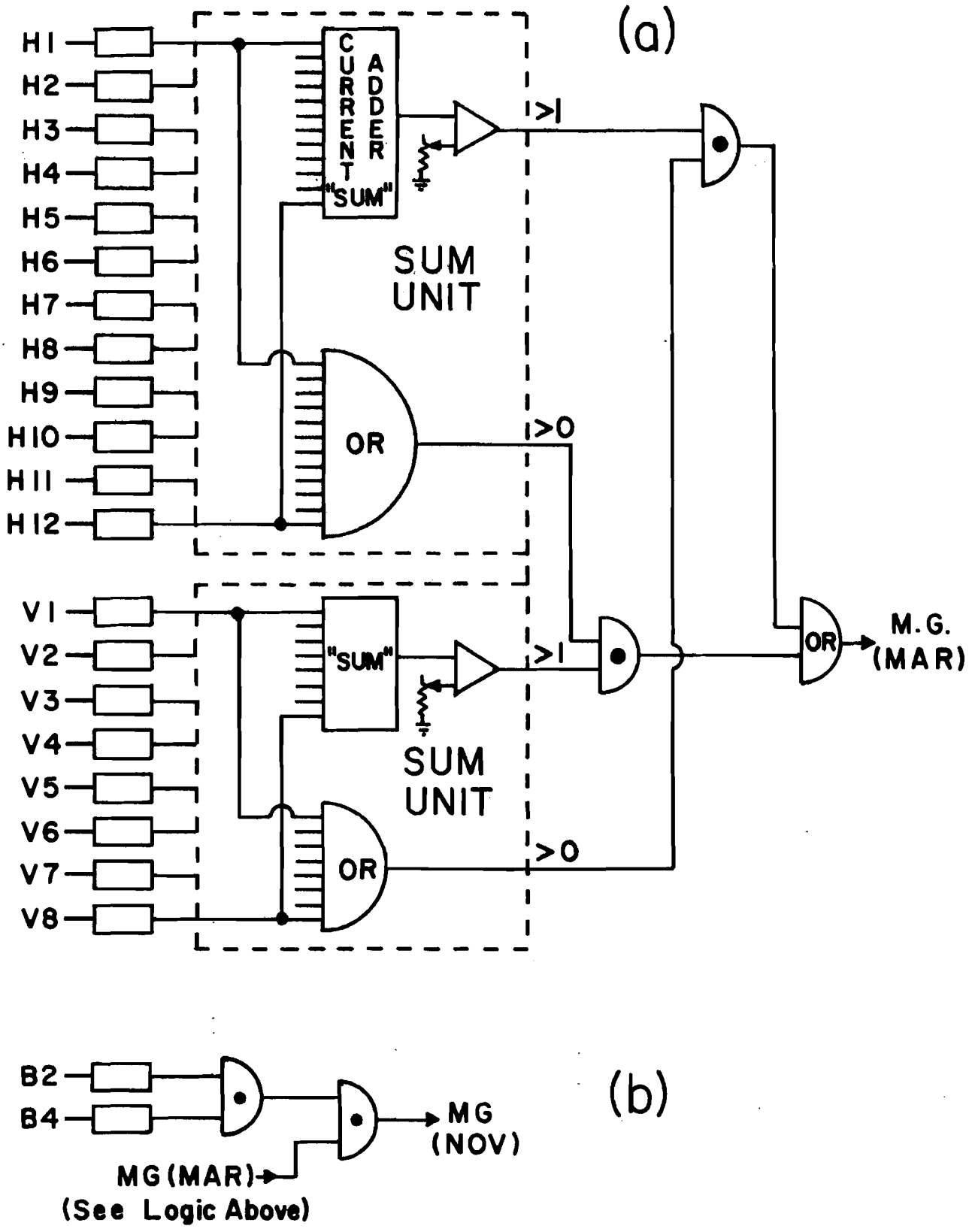

Figure 8. Master gate logic: (a) the (H, V>1) logic for the master gate in the March run; (b) the additional logic required for the master gate in the November run.

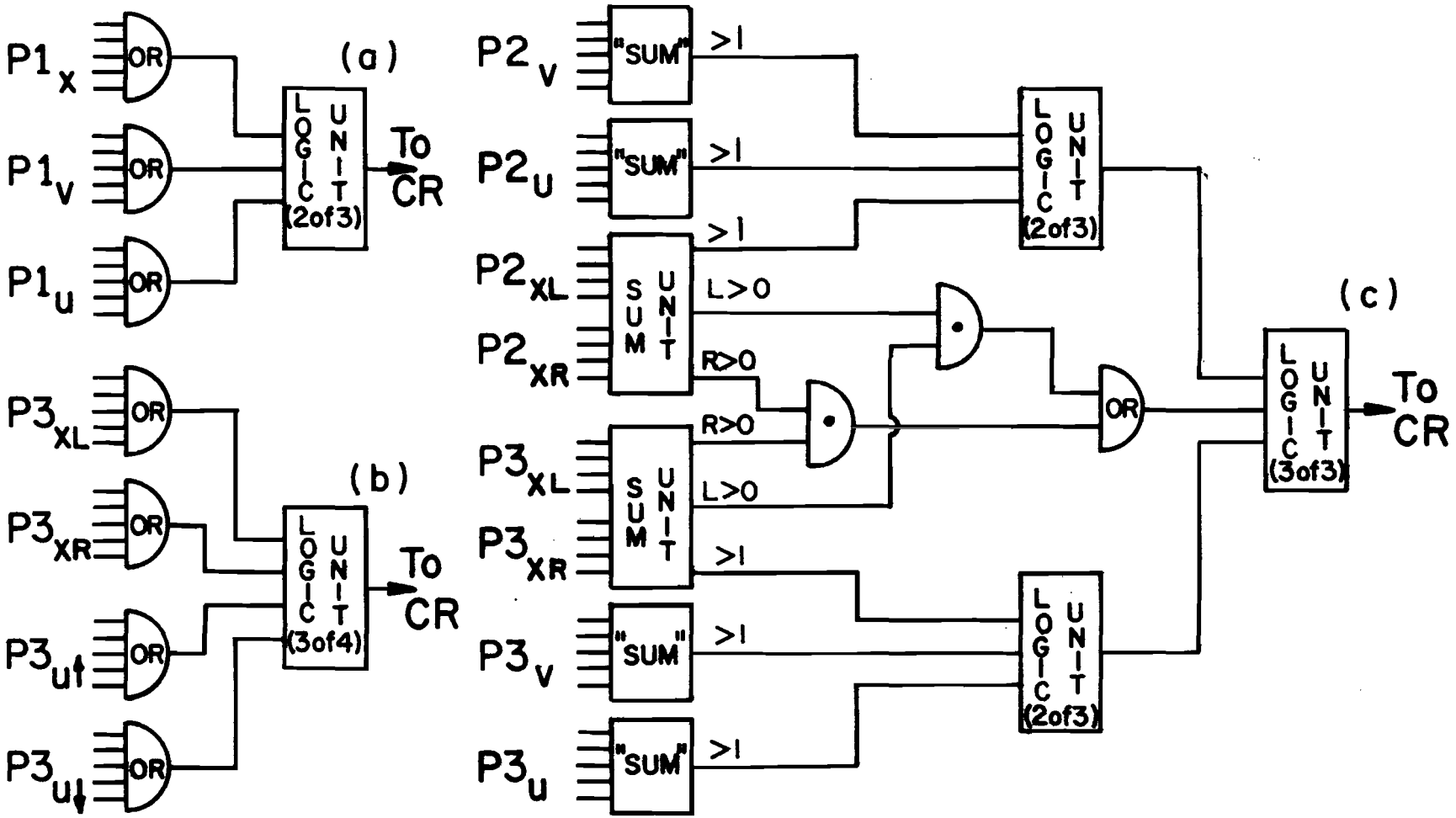

Figure 9. MWPC logic: (a) the P1 logic for both runs (b) the P3 logic for the November run (c) the wide angle track logic for the March run

The inputs to the coincidence registers were discriminator signals from some part of the counter system and outputs from earlier logic such as the MWPC logic. The outputs included one for each register and a "sum" output for each group of four registers. Each register that was set added 4 ma to the appropriate sum output.

Sum logic modules accepted up to eight sum signals from coincidence register modules and summed the currents. The current information was then converted to voltage and compared with three reference levels to define >0, >1, and >2 levels. Further logic provided several outputs including those corresponding to the levels $(=0)$, (>0), and (>1).

In the CR logic, shown in figure 10, sum logic modules were used to determine the number of hits in each plane of arrays of horizontal and vertical counters. A H x V module accepted the sum logic module outputs for the horizontal and vertical planes of an array and determined the number of tracks in that array. With the inputs used, the outputs (0), (1), and (2) corresponded to $=0$, >0, and >1 tracks respectively. The L x R module accepted the H x V outputs for arrays to the left and right of the beam line and generated outputs for specific event type classifications.

Figure 10a shows this logic as it was used to generate the ≥ 2 tracks, symmetric ≥ 2 tracks, and asymmetric ≥ 2 tracks bus lines from the (H, V) counter information. The symmetric ≥ 2 muons and

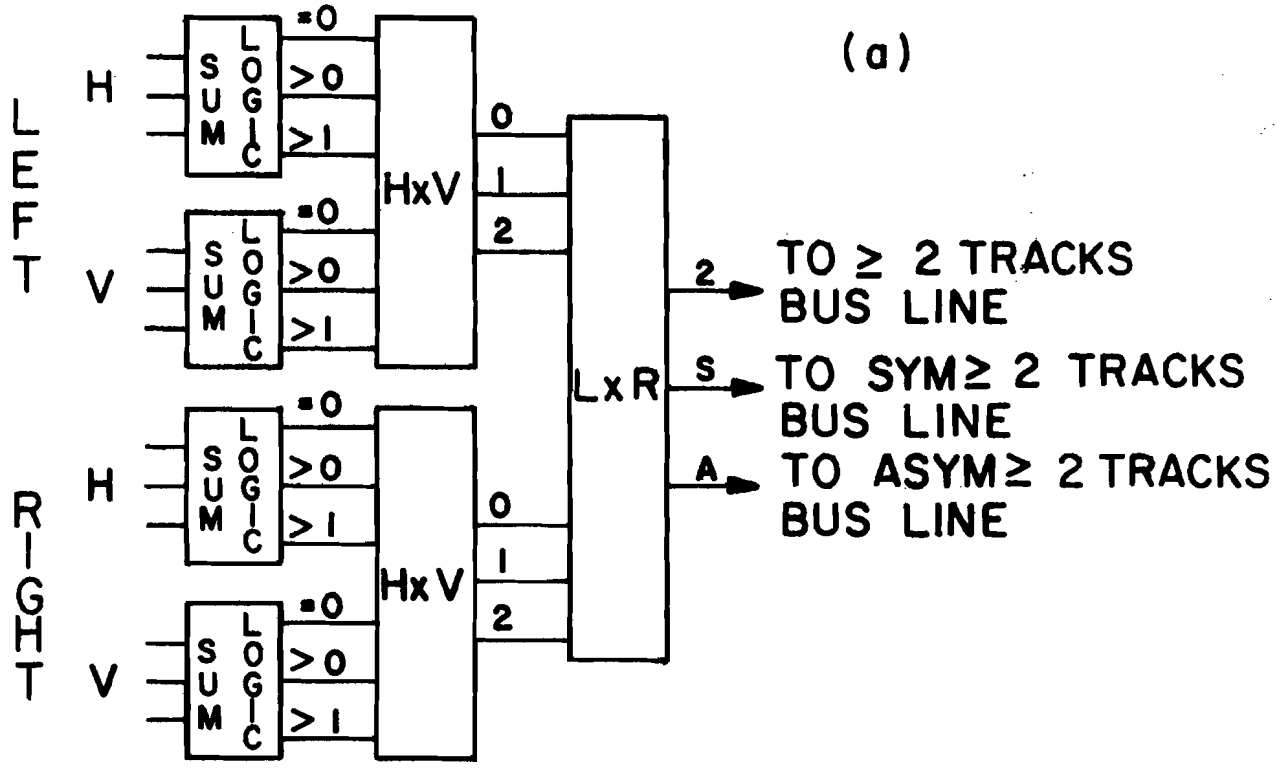

V \ H	=0	>0	>1
=0	0	0	
>0	0	1	2
>1		2	2

HxV LOGIC

R \ L	0	1	2
0			2
1		2	
2	2		

R \ L	0	1	2
0			A
1		S	
2	A		

LxR LOGIC

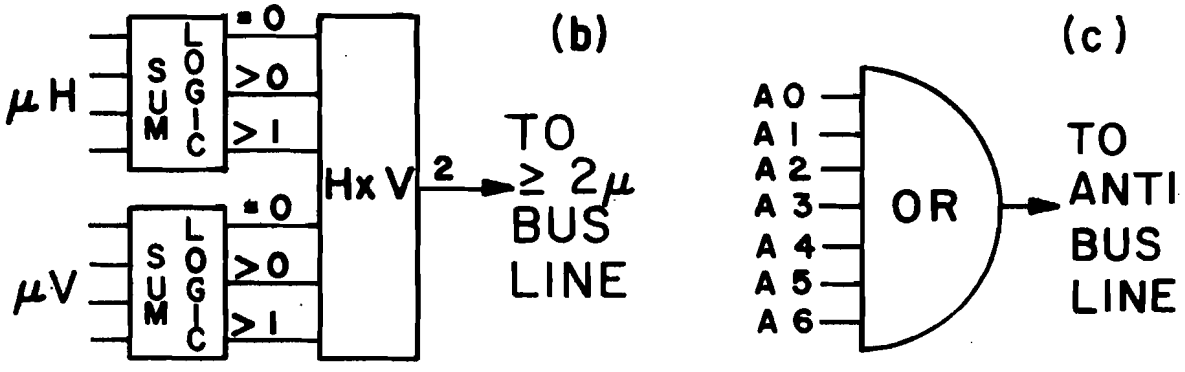

Figure 10. Coincidence register (CR) logic: (a) the "two track" logic and logic tables for the H x V and L x R modules; (b) the "any two muons" logic; (c) the anti-counter logic

asymmetric $\geq$ 2 muons bus lines were generated in the same manner from the muon counter information. A less restrictive $\geq$ 2 muons bus line was generated as shown in figure 10b. Figure 10c shows the logic used to generate the anti-counter bus line. The bus lines for the B counters and the MWPC logic were generated from the appropriate coincidence register outputs with no further logic required.

Output triggers were generated in the pin logic system as indicated in figure 11. Listed are all the bus lines that were used and their status as required for each event type. For a given pin logic each bus line was required to be true (✓), required to be false (X), or ignored. The event triggers were symmetric two muons and asymmetric two muons for the November run and any two muons for the March run.

BUS LINES	PIN LOGIC		
	ANY 2μ	SYM 2μ	ASYM 2μ
≥ 2 TRACKS	✓		
SYM ≥ 2 TRACKS		✓	
ASYM ≥ 2 TRACKS			✓
≥ 2 MUONS	✓		
SYM ≥ 2 MUONS		✓	
ASYM ≥ 2 MUONS			✓
B 3	✓		
B 4		✓	✓
MWPC-P1 (2 of 3)	✓	✓	✓
MWPC-P3 (3 of 4)		✓	✓
MWPC-WIDE TRACK	✓		
ANTI	X	X	X

Figure 11. Pin logic table

III. ANALYSIS

A. Data Reduction

During the two runs approximately 1.4 million events were accepted and written on magnetic tape. The data were reconstructed on the CDC 6600 computer at Fermilab. The first step in the data reduction process, also done on the Fermilab CDC 6600 computer, was to eliminate all events with less than two reconstructed tracks. The output tapes were written so as to be compatible with the DEC PDP-10 computer facility at the University of Illinois. All further data processing was done at the University of Illinois.

The next step in the condensation process eliminated events with less than two muon candidates. A muon candidate was required to project to within the radius of search of at least one muon counter that was on. See section III-B for a description of the muon identification.

Finally, a series of cuts on the quality of the event reconstruction were made. No proportional wire address was allowed to be used for more than two tracks, and no more than three addresses could be used more than once. The calculated momentum of a track was required to be between 5 GeV/c and 300 GeV/c. A very loose cut on the mean squared deviation of the reconstruction fit was also made.

A final vertex cut was made to reduce further the data to approximately one tape per run. This cut required the apparent vertex to be at least a few decimeters upstream of the absorber. A tighter target

cut was required in the final analysis to get a clean separation of the target and absorber for high mass pairs.

In the final analysis the momentum weighted position between the muons at the target was required to be within 5 cm, horizontally and vertically, of the beam line. A cut was also applied to the distance of nearest approach weighted by the function, $pq/(p+q)$, where p and q are the momenta of the two muons. For a 100 GeV dimuon whose energy is shared equally by the two muons, this cut required the distance of nearest approach to be less than 3.0 cm for the November run and less than 2.5 cm for the March run.

A target cut was made which required the dimuon vertex to be within 75 cm of the target for the November run and within 60 cm of the target for the March run. This target cut was chosen for each run to provide the best separation of the target and absorber for the high mass dimuons.

B. Muon Identification

The identification of muons was done by projecting the track to the μ H and μ V counter planes and requiring that the appropriate counters be on. The projected position of the track in each plane was required to be within and at least 5 cm from the outer boundaries of that plane. If the counter to which the track projected was not on, adjacent counters within a given radius were also examined. The radius of search was inversely proportional to the momentum and corresponded to a distance of three times the rms projected dis-

placement expected from multiple scattering as calculated in an uniform absorber approximation. If the calculated radius was greater than 10 cm, it was set equal to 10 cm (half a counter width).

Each track was tagged with the number of muon counters which could be associated with that track. A muon candidate was required to have at least one counter associated with it. Dimuon events were required to have at least three counters associated with the two tracks. Tracks were allowed to share counters.

C. Mass Calculation

For large momenta and small opening angle, the invariant mass M of a muon pair can be expressed in the form:

$$M^2 = m^2(2 + p/q + q/p) + pq\theta^2$$

where m is the muon mass, p and q are the muon momenta, and θ is the opening angle of the muons. The momenta were measured in the magnetic spectrometer and corrected for the energy loss in the absorber.

The mass resolution for muon pairs is appreciably worsened by the multiple scattering in the absorber. However, some improvement can be made by recalling that the position at which a muon leaves an absorber is less affected by multiple scattering than is the angle at which it leaves. Furthermore, since the changes in position and angle due to the multiple scattering are correlated, a better estimate of a point on the "unscattered" trajectory of the muon can be made by projecting the track back into the absorber.

The opening angle of the muon pair was calculated by projecting the tracks back into the absorber and assuming the pair originated in the target. In general, the "best" position in the dump for calculating opening angles depends on the position of the target, the angular resolution of the magnetic spectrometer, and the distribution of the material in the absorber. However, the minimum in the angular uncertainty is a relatively broad minimum, and the mass resolution is not a strong function of the precise position in the absorber used to calculate the opening angles.

For masses greater than about 1 GeV/c^2, our resolution in the position of nearest approach was sufficient to separate pairs produced in the target from those produced in the absorber. Therefore, dimuons from the absorber represent a significant background only for the very low mass region of the spectrum since mistakenly assuming a dimuon from the absorber was produced in the target appreciably underestimates its mass.

Since there were no significant upstream sources of dimuons, the only potentially troublesome muon pairs which could erroneously give large masses by this calculation were those where the muons were appreciably separated spatially. These were probably uncorrelated muons and were easily eliminated with rather loose cuts on the distance of nearest approach and/or the separation at the target.

D. Monte Carlo Event Simulation

The data were compared with simulated events generated with distributions of the form:

$$\frac{d^2N}{dP_{\parallel}\, dP_{\perp}^2} \propto \exp(-\alpha P_{\parallel}) \exp(-\beta P_{\perp}^2)$$

Discrete dimuon masses were used for particles whose widths are much smaller than the mass resolution of the detector. For broad resonances, the masses were generated with symmetric Briet-Wigner distributions. Center of mass decay distributions were generated with uniform, $1 + \cos^2\theta^*$, and $\sin^2\theta^*$ distributions where θ^* is the angle of the muon relative to the dimuon direction. For most of the acceptance calculations, the isotropic decay distribution was used.

The generated muons were multiple scattered through the absorber and corrected for the energy lost in the absorber with Monte Carlo simulations of these processes. Effects of the spectrometer resolution were considered by projecting each track to the proportional chambers, converting the projected positions to wire addresses, and reconstructing the track vector from these addresses. Each generated event was required to pass the appropriate plane cuts for that run and to satisfy the corresponding MWPC logic.

The parameters α and β were varied until the simulated events, after propagation through the apparatus, produced distributions that were consistent with the experimental distributions. These values of

the parameters were then used for the acceptance calculations.

E. Normalization

Normalizations for the cross section calculations were obtained by determining the number of target interactions for each run and assuming a neutron cross section of 210 mb per nucleus. With this normalization, the product of the production cross section (σ), branching ratio into muon pairs (B), and acceptance (A) is $\sigma \cdot B \cdot A = (N/N_I) \cdot 210$ mb/nucleus, where N is the number of observed events, and N_I is the effective number of neutron interactions in the experimental target.

For the November run with the segmented target configuration, the counter (B1) between the two targets recorded the number of interactions in the upstream target. Corrections were made for the "target empty" rate from the data taken without this upstream target. The number of interactions in the upstream target was scaled by the ratio of the effective target lengths to get the number of interactions in the full target.

For the March run the number of target interactions was measured directly with the trigger counter B3. A run with no target provided the "target empty" correction. A preliminary determination of the number of neutrons in the neutral beam per incident proton has also been made for this run from the neutron spectrum data. These two flux determinations agree to better than 20%.

The data were checked for internal consistency by comparing the yields for different subsets of data. Yields for the rho region, the J/psi region, and the "Drell-Yan" region (between 1.4 and 2.4 GeV/c^2) were compared for different target thicknesses for the November run and for each combination of target thickness and magnet polarity for the March run. There were indications of possible systematic effects at the level of 10 to 20% in the March run. From a study of these yields, we believe that we have determined the relative normalization within each run to better than 15% for the November run and 25% for the March run.

The systematic uncertainty introduced by the Monte Carlo calculation of the acceptance is estimated to be less than 20%. Uncertainties in the true production and decay distributions of the dimuons introduce additional uncertainties in the calculated acceptances. Cuts on the longitudinal momenta of the observed dimuons help reduce these uncertainties to reasonable levels in comparison to the other experimental uncertainties.

Other systematic uncertainties are more difficult to estimate. Some of the more serious of these are probably due to the proton beam r.f. structure and spill quality, the targeting efficiency, and the photon and other low energy components of the neutral beam.

Including estimates of the systematic errors, we believe the measured cross sections are correct within a factor of two.

F. Drell-Yan Calculation

In the Drell-Yan mechanism for massive dimuon production, the pair is created by the parton-antiparton annihilation process. A parton (antiparton) moving to the right with a fraction X_1 of the momentum of one nucleon annihilates with an antiparton (parton) moving to the left with a fraction X_2 of the momentum of the other nucleon producing a dimuon of mass M and longitudinal momentum p^*. Including a factor of 1/3 for color, the standard Drell-Yan formula for this process at very high center of mass energy $\sqrt{S}$ is:[12]

$$\frac{d\sigma}{dMdp^*} = 2M \cdot \frac{1}{3} \cdot \int \frac{dX_1}{X_1} \int \frac{dX_2}{X_2} \cdot \frac{4\pi\alpha^2}{3M^2} \cdot G(X_1, X_2) \cdot$$
$$\delta(M^2 - X_1 X_2 S) \cdot \delta(p^* - (X_1 - X_2) \cdot \sqrt{S}/2)$$

where

$$G(X_1, X_2) = \sum_i e_i^2 (f_i(X_1)\, f_i(X_2) + f_i(X_2)\, f_i(X_1))$$

The sum is over partons of type i having a charge e_i and density function f_i. After integration:

$$\frac{d\sigma}{dMdp^*} = 2M \cdot \frac{1}{3} \cdot \frac{4\pi\alpha^2}{3M^4} \cdot S^{-1/2}(p^{*2} + M^2)^{-1/2} \cdot G(X_A, X_B)$$

where

$$2X_{A,B} = (X_F^2 + 4M^2/S)^{1/2} \pm X_F \quad \text{and } X_F = 2p^*/S$$

This equation was then integrated numerically to get the appropriate predicted distributions. The parton distribution functions used in the numerical integration are those given by Blankenbecler, et al.[13]

IV. RESULTS

A. Mass Distributions

Mass distributions are presented for oppositely charged dimuons with total energy greater than 40 GeV. To be included in these mass plots, the event was required to pass all the event cuts described in section III-A including the target cut that best separates the target and absorber for the high mass pairs. Although this target cut is strongly mass dependent for low mass dimuons, it does not change the general features of the data.

Figure 12 shows the mass distributions for masses less than 1.4 GeV/c^2. The dominant features of this data are the presence of the clear peak in the region of the rho mass and the presence of a dimuon continuum that peaks at low mass and falls off with increasing mass. There are also indications of a shoulder in the mass distribution in the region of 1.0 GeV/c^2 which suggests the presence of a phi meson signal.

The large enhancement in the rho mass region clearly represents the production of the rho and omega mesons in the target. Our mass resolution, however, does not allow us to distinguish the rho from the omega. Although any omega production would be included in this peak, this enhancement will be referred to as the rho meson. Any rho production in the absorber would be included in the low mass peak.

Figure 12. Invariant mass distributions below 1.4 GeV/c^2 for oppositely charged muon pairs: (a) November run; (b) March run

Figure 13 shows the mass distributions for masses greater than 1.4 GeV/c^2. We observe a dimuon continuum that continues to fall rapidly with increasing mass and an obvious peak at 3.1 GeV/c^2 whose width is consistent with our experimental resolution. We associate this enhancement at 3.1 GeV/c^2 with the narrow resonance observed in nucleon-nucleon interactions[6] and electron-positron annihilations.[7]

We define the J/psi(3100) to be any event between 2.7 GeV/c^2 and 3.5 GeV/c^2. In this mass interval we have observed fifty-five events in the November run and fifty events in the March run. The longitudinal and transverse distributions for these events are discussed in the next section.

Two potentially troublesome backgrounds which must be considered, especially in any discussion of the dimuon continuum, are decays in flight and dimuons produced in the absorber. Since, in general, decays in flight are expected to produce uncorrelated muons, one expects roughly comparable numbers of charge two and charge zero pairs from this source. Therefore, the distribution of charge two muon pairs should be indicative of the dimuon background due to decays in flight.

Figures 14a and 14b show the mass distributions of like charged muon pairs with the same event cuts as used for the oppositely charged pairs. Below 1.15 GeV/c^2 the ratio of like charged muon pairs to oppositely charged pairs is less than 10% for all mass bins. Between 1.2 and 2.0 GeV/c^2 this ratio is about 20% with low statistics. There

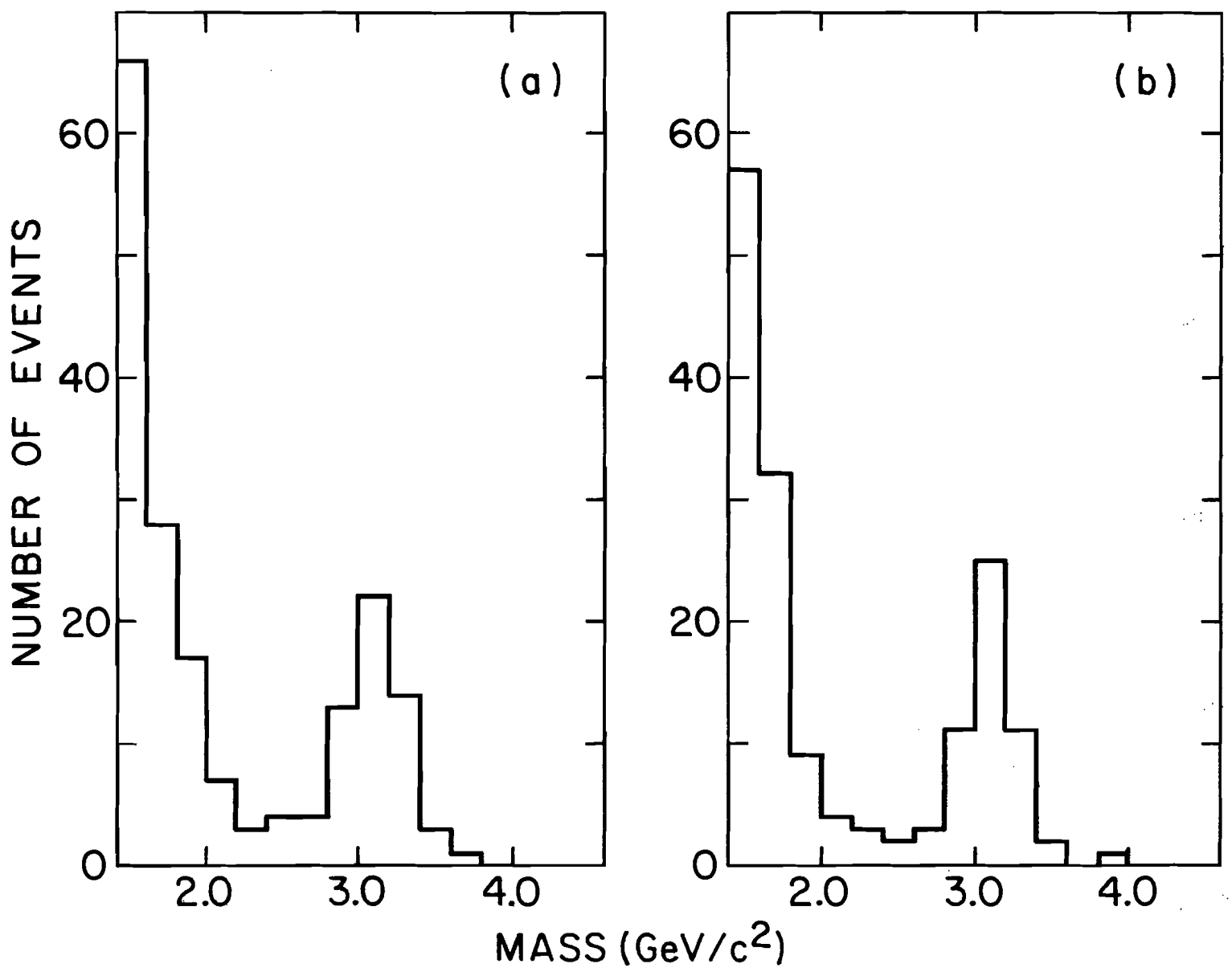

Figure 13. Invariant mass distributions above 1.4 GeV/c^2 for oppositely charged muon pairs: (a) November run; (b) March run

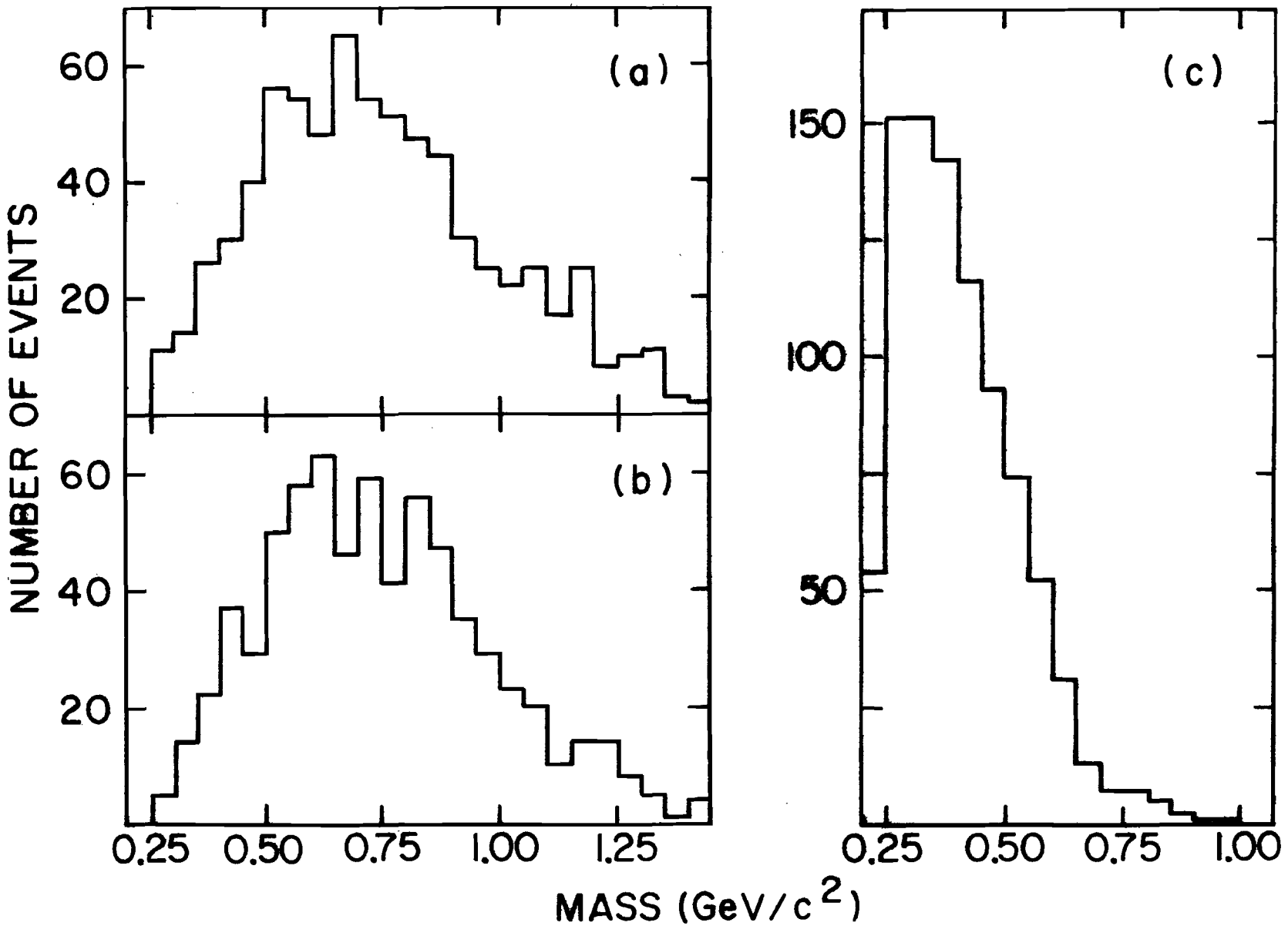

Figure 14. Invariant mass distributions: (a) and (b) for like charged muon pairs, (a) November run, (b) March run; (c) for dimuons produced in the absorber but assumed to come from the target

are no like charged muon pairs above 2.2 GeV/c^2.

Figure 14c shows the mass distribution for dimuons produced in the absorber for which the mass was calculated assuming the pair was produced in the target. We see that the distribution is very strongly peaked toward low masses, presenting a rather severe background for masses below the rho region. For masses above 1 GeV/c^2 the absorber is a negligible source of dimuons since the resolution in vertex position is sufficient to eliminate the high mass pairs from the absorber that would give calculated masses in this region.

B. J/Psi(3100)

The longitudinal momentum distributions for the events in the J/psi region are shown in figure 15. The curves are the predicted distributions calculated by the Monte Carlo program for simulated events generated with the indicated distributions. We see that the data are consistent with the distributions shown. The experimental distributions are corrected for acceptance and shown in figure 16. The errors shown are statistical only.

The data are consistent with a longitudinal momentum distribution of the form $\exp(-\alpha P)$ with:

$$\alpha = \begin{cases} 0.04 & \text{(November run)} \\ 0.03 & \text{(March run)} \end{cases}$$

If α is expressed in the form $\alpha = \alpha'/p_n$ where p_n is the mean incident neutron momentum in the laboratory, we find that our data

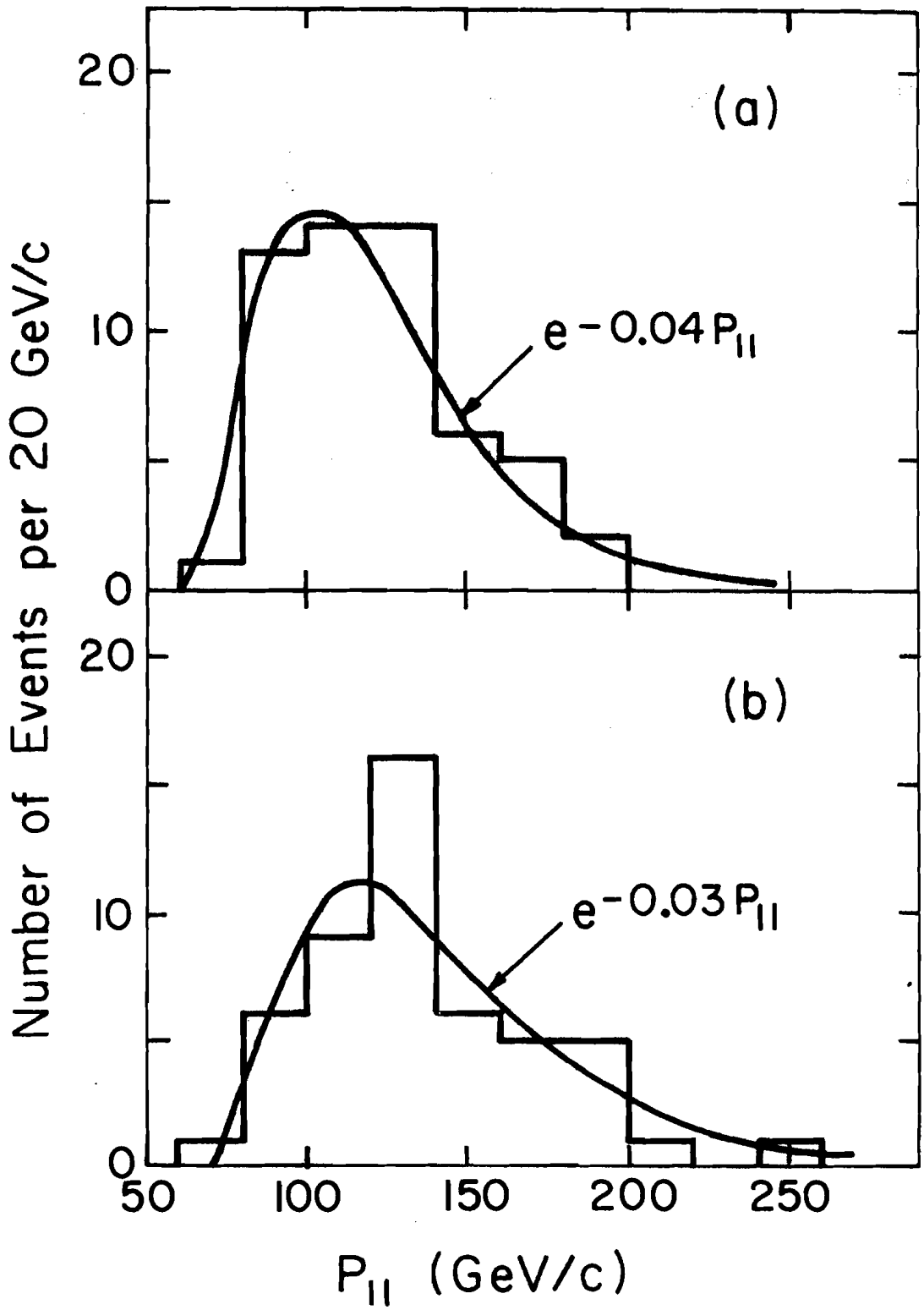

Figure 15. Longitudinal momentum distributions: (a) November run; (b) March run. The curves are the calculated distributions for simulated events generated with the indicated distributions.

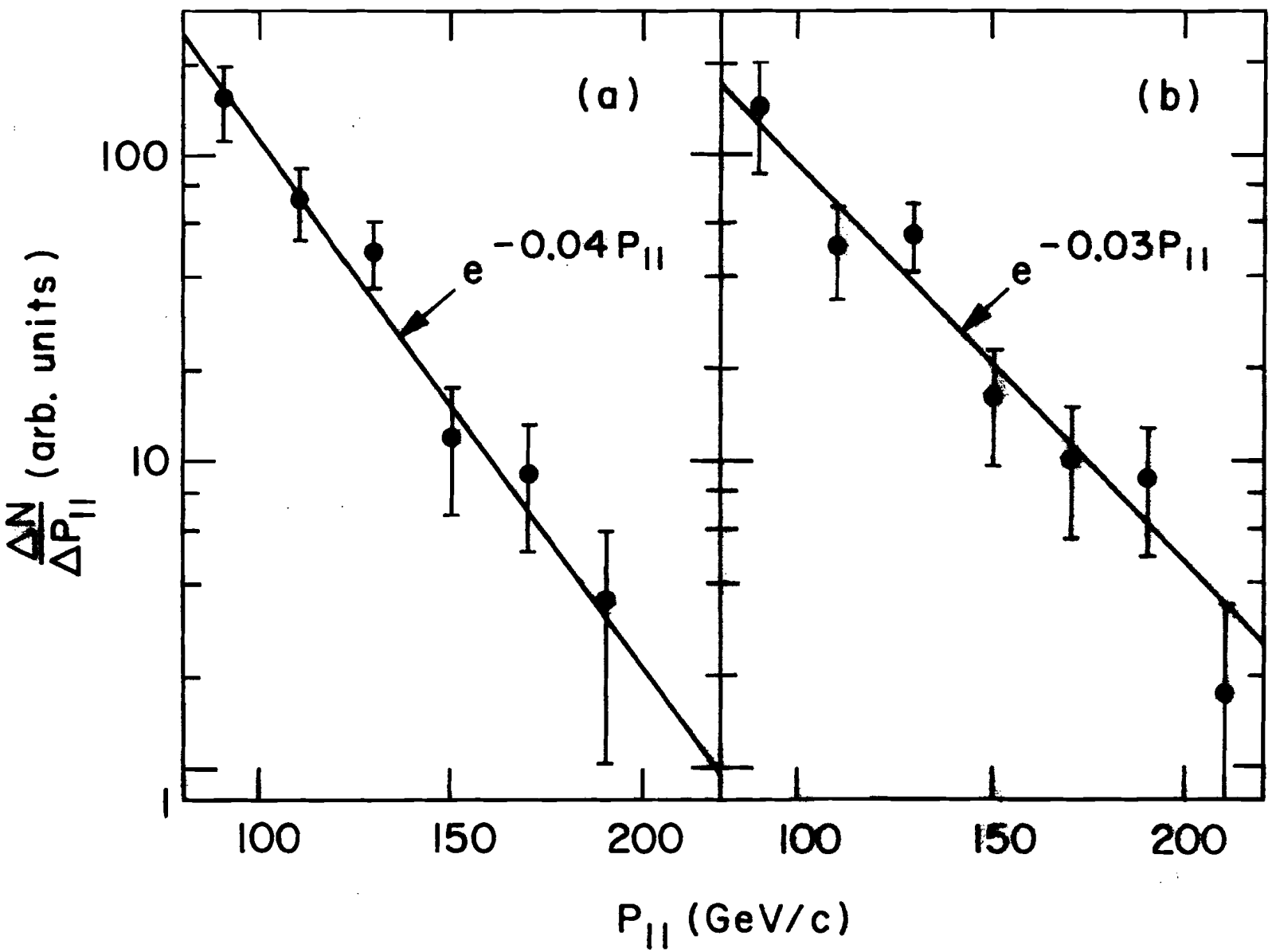

Figure 16. Longitudinal momentum distributions corrected for the acceptance of the apparatus: (a) November run; (b) March run. The errors shown are statistical only.

are consistent with $\alpha' = 10$. This corresponds to a longitudinal momentum distribution of the form $\exp(-10X_L)$ where X_L is the ratio of the dimuon longitudinal momentum to the incident neutron momentum in the laboratory. X_L is related to the usual center of mass X_F by $X_F = X_L - M^2/(X_L \cdot S)$ where M is the dimuon mass.

The transverse momentum distributions for the events in the J/psi region are shown in figure 17. The data has been corrected for acceptance (uniform within $\sim$10%), and the errors shown are statistical only.

In figure 17a the data have been plotted as a function of $P_\perp^2$. The data are in bins 0.2 $(GeV/c)^2$ wide selected so that the data points of one run lie between those of the other run. The relative normalization of the two runs has been adjusted to allow a direct comparison of the two distributions. We see no evidence for any energy dependence of the transverse momentum distribution of the J/psi. The data are consistent with a distribution of the form $\exp(-1.25P_\perp^2)$.

The data from the two runs are combined, and $\Delta N/\Delta P_\perp^2$ is plotted as a function of $P_\perp$ in figure 17b. The data are consistent with a distribution of the form $\exp(-1.5P_\perp)$.

With the fifty-five events in the November run and the fifty events in the March run in the J/psi mass region (2.7 GeV/c^2 to 3.5 GeV/c^2); the product of cross section, branching ratio into muon pairs, and

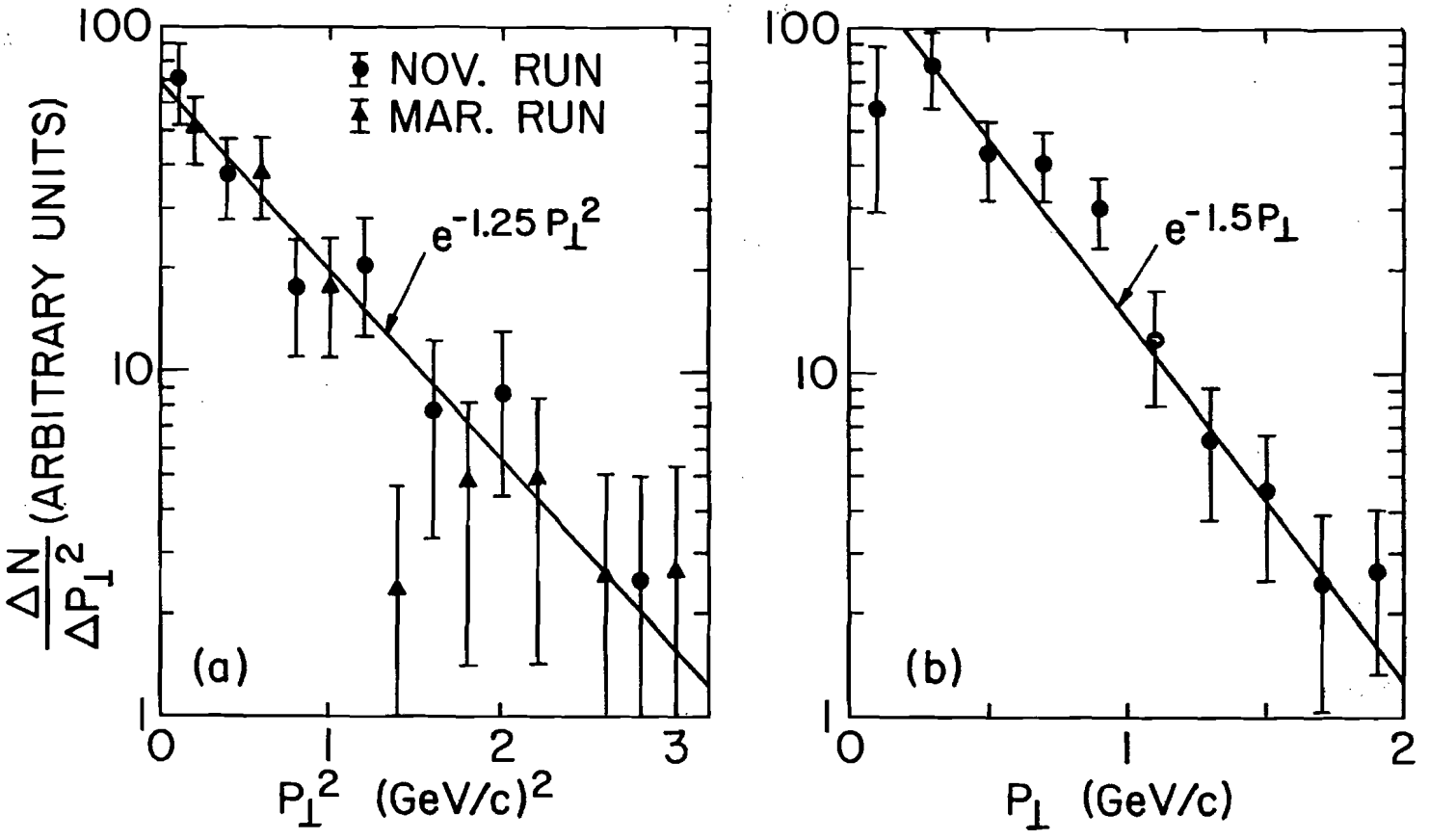

Figure 17. Transverse momentum squared distributions corrected for the acceptance of the apparatus as functions of: (a) the transverse momentum squared; (b) the transverse momentum. The data from the two runs have been combined for figure (b). The errors shown are statistical only.

acceptance of the apparatus is:

$$\sigma \cdot B \cdot A = \begin{cases} 0.92 \text{ nb/nucleus} & \text{(November run)} \\ 1.80 \text{ nb/nucleus} & \text{(March run)} \end{cases}$$

Correcting for acceptance, the cross sections times branching ratio are:

$$\sigma \cdot B = \begin{cases} 11.1 \text{ nb/nucleus, } P > 60 \text{ GeV/c} \\ 5.2 \text{ nb/nucleus, } P > 80 \text{ GeV/c} \end{cases} \quad \text{(November run)}$$

$$\sigma \cdot B = \begin{cases} 11.4 \text{ nb/nucleus, } P > 75 \text{ GeV/c} \\ 5.4 \text{ nb/nucleus, } P > 100 \text{ GeV/c} \end{cases} \quad \text{(March run)}$$

Although the acceptances of the experiments are quite different, it is clear that this cross section is much larger than that reported by the BNL experiment.[6] These results are consistent with those recently reported by other Fermilab experiments.[14, 15]

Using our parameterization of the data to extrapolate our result to $X_F = 0$, we obtain a cross section:

$$\frac{d\sigma}{dX_F} \cdot B \Big|_{X_F = 0} = 170 \text{ nb/nucleus} = 19 \text{ nb/nucleon}$$

Expressed in terms of rapidity, this result is:

$$\frac{d\sigma}{dy} \cdot B \Big|_{y = 0} = 45 \text{ nb/nucleus} = 5 \text{ nb/nucleon}$$

This is consistent with the cross section measured at the ISR for J/psi production.[16]

C. Dimuon Continuum

Figure 18 shows the dimuon cross section as a function of dimuon mass between 1.0 GeV/c^2 and 3.0 GeV/c^2 for X_L greater than about 0.24 (momenta above 60 GeV/c for the November run and above 75 GeV/c for the March run). The data are plotted in 0.2 GeV/c^2 bins selected so that the data points of one run lie between those of the other run. The errors shown are statistical only.

The curve is the prediction of the Drell-Yan model with color calculated as described in section III-F. Except for the tail of the rho and possible phi production at the lower masses and the J/psi at the higher masses, the data is consistent with the Drell-Yan prediction. Given the uncertainty in the absolute normalization of the data, the agreement is remarkable, especially in the region where there are no known vector mesons and the backgrounds are known to be small.

It should be noted that the events in this mass region may be produced by entirely different processes.

D. Psi'(3700)

There are two events above the J/psi region that have masses consistent with that of the psi'(3700). However, other possible sources for these events include the tail of the J/psi and the high mass dimuon continuum.

From our data we estimate that in the region above 3.6 GeV/c^2, there should be less than 0.4 events from the J/psi and 1.0 to 1.8

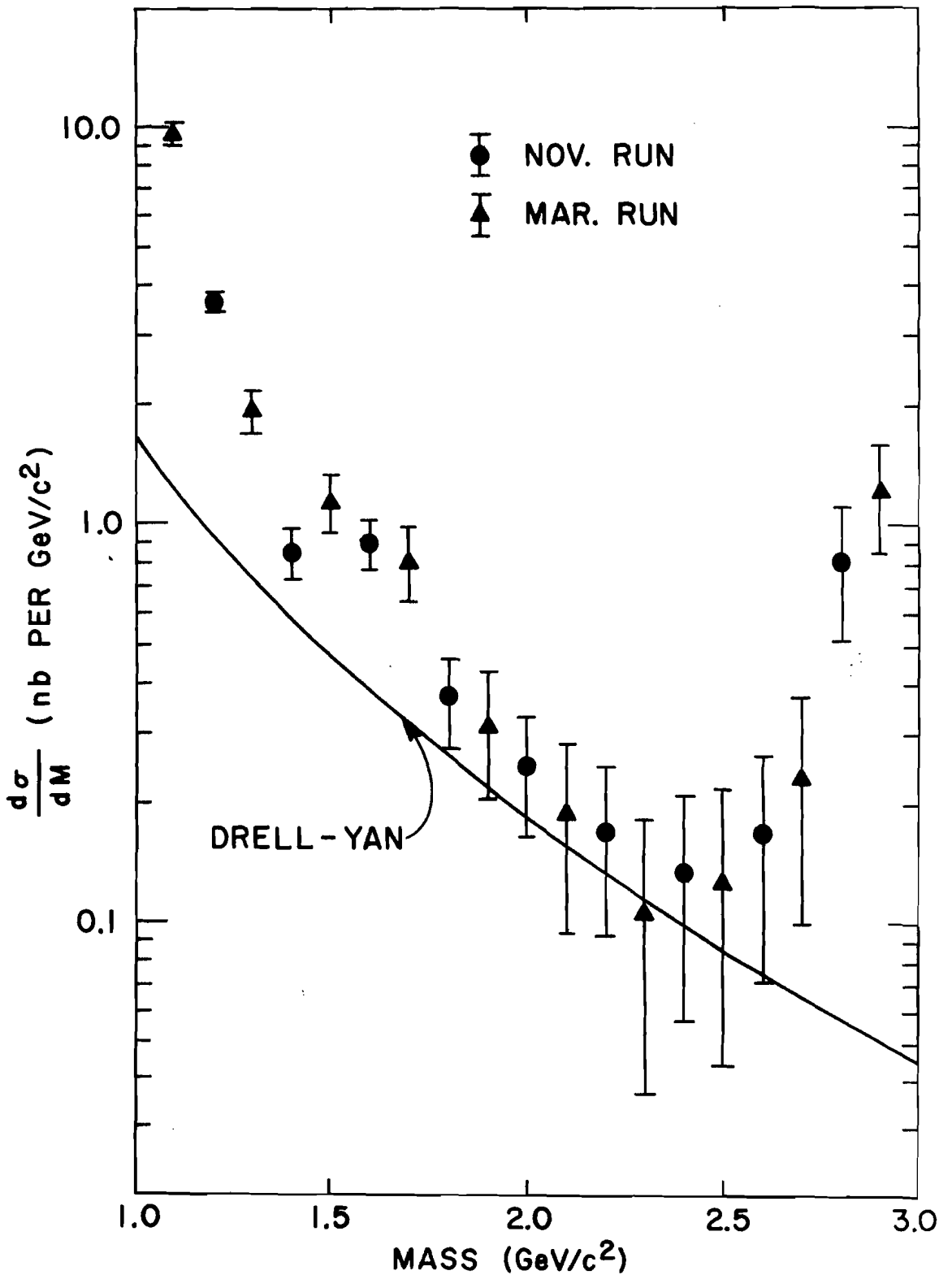

Figure 18. The dimuon cross section as a function of dimuon mass for $X_L > 0.24$. The curve is the prediction of the Drell-Yan model with color. The errors shown are statistical only.

events from the continuum. This is certainly consistent with the data. Therefore, we conclude that there is no clear evidence for psi' production in this experiment.

With the acceptance a factor of 0.6 lower and the branching ratio a factor of 0.14 lower for the psi' than for the J/psi, the ratio of the cross section for the psi' to that of the J/psi is $\sim$12 times the ratio of the events observed.

Assuming that the two events are background events and do not represent psi' production, an upper limit of 0.26 (90% confidence level) is obtained for the ratio of psi' to J/psi production. However, if the two events are psi' events, then the ratio of psi' to J/psi production is 0.23 ± 0.16.

V. SUMMARY

The dimuon production by high energy neutrons has been measured for incident neutron energies of approximately 250 and 320 GeV. Cross sections for the two energies are consistent with a flat energy dependence.

The mass spectra show clear peaks in the rho mass region and at the J/psi mass with a dimuon continuum between them.

The measured J/psi cross sections are:

$$\sigma \cdot B = \begin{cases} 11.3 \text{ nb/nucleus} = 1.25 \text{ n/nucleon for } X_L > 0.24 \\ 5.3 \text{ nb/nucleus} = 0.59 \text{ n/nucleon for } X_L > 0.32 \end{cases}$$

These cross sections are clearly much larger than observed at BNL energies but are in reasonable agreement with other results from Fermilab and the ISR.

The J/psi data has been compared with Monte Carlo generated events of the form $\exp(-\alpha X_L) \exp(-\beta P_\perp^2)$. The data are consistent with $\alpha \approx 10$ and $\beta \approx 1.25$.

The data between the rho mass region and the J/psi have been compared with the prediction of the Drell-Yan model. The data are found to be remarkably consistent with the predicted distribution in the region where there are no known vector mesons.

Finally, the data are consistent with no psi'(3700) production in this experiment.

REFERENCES

1. B. Knapp et al., Phys. Rev. Lett. 34, 1044 (1975).
2. J. P. Boymond et al., Phys. Rev. Lett. 33, 112 (1974).
3. J. A. Appel et al., Phys. Rev. Lett. 33, 722 (1974).
4. F. W. Busser et al., Phys. Lett. 53B, 212 (1974).
5. L. B. Leipuner et al., Phys. Rev. Lett. 34, 103 (1975).
6. J. J. Aubert et al., Phys. Rev. Lett. 33, 1404 (1974).
7. J. E. Augustin et al., Phys. Rev. Lett. 33, 1406 (1974).
8. C. Bacci et al., Phys. Rev. Lett. 33, 1408 (1974).
9. G. S. Abrams et al., Phys. Rev. Lett. 33, 1453 (1974).
10. The production of the dimuon continuum was first reported by Christenson et al., Phys. Rev. Lett. 25, 1523 (1970); Phys. Rev. D 8, 2016 (1973).
11. S. D. Drell and T. M. Yan, Phys. Rev. Lett. 25, 316 (1970); Ann. Phys. (N. Y.) 66, 578 (1971).
12. See, for example, J. D. Bjorken and H. Weisberg, unpublished report to the International Conference on High Energy Physics, Palermo, Italy (1975).
13. R. Blankenbecler et al., SLAC-PUB-1531, 1975 (unpublished).
14. G. J. Blanar et al., Phys. Rev. Lett. 35, 346 (1975).
15. J. Pilcher, preliminary unpublished results presented at the 1975 International Symposium on Lepton and Photon Interactions at High Energies, Stanford, California (1975).
16. F. W. Busser et al., Phys. Lett. 56B, 482 (1975).

VITA

Clyde Dean Wheeler was born in Mangum, Oklahoma, on January 1, 1938. He attended public school in Martha, Oklahoma, and received his high school diploma from Martha High School in 1956. He received the B.S. degree (magna cum laude) from Southwestern State College, Weatherford, Oklahoma, in 1960. In 1960-1961 he attended graduate school at the University of Pittsburgh where he held a teaching assistantship.

He taught physics at Southwestern State College for seven of the years between 1961 and 1969. During 1965-1966 he attended a National Science Foundation Academic Year Institute for College Teachers at Cornell University where he received the M.S.T. degree in 1966.

He entered the graduate school at the University of Illinois in 1969 and received the M.S. degree from that institution in 1971. Since 1969 he has held teaching and research assistantships in the Physics Department. During 1970-1971 he was awarded the Eastman Kodak Industrial Fellowship.

He is co-author of the papers "Photoproduction of Narrow Resonances," Phys. Rev. Lett. 34, 1040 (1975) and "Dimuon Production by Neutrons," Phys. Rev. Lett. 34, 1044 (1975).